EasyChair Preprint

№ 2399

Temperature Measurement of a Turbulent Buoyant Ethylene Diffusion Flame Using a Dual-Thermocouple Technique

Xingyu Ren, Dong Zeng, Yi Wang, Gang Xiong, Gaurav Agarwal and Michael Gollner

January 17, 2020

Temperature measurement of a turbulent buoyant ethylene diffusion flame using a dual-thermocouple technique

Xingyu Ren[a], Dong Zeng[b*], Yi Wang[b], Gang Xiong[b], Gaurav Agarwal[b], Michael J. Gollner [a,c*]

[a]Department of Fire Protection Engineering, University of Maryland, College Park, MD, USA,

[b]Research Division, FM Global, 1151 Boston-Providence Turnpike, Norwood, MA 02062, USA, dong.zeng@fmglobal.com

[c]Department of Mechanical Engineering, University of California, Berkeley, CA, USA
[*]mgollner@berkeley.edu

Highlights:

- A temperature dataset is established for a buoyant turbulent ethylene flame.
- A dual-thermocouple technique is used to compensate turbulent gas temperatures.
- Mean, root-mean square and probability density function temperatures are provided.

Abstract:

High-frequency temperature measurements were carefully conducted for a 15 kW buoyant turbulent ethylene diffusion flame over a 15.2 cm diameter gas burner with air co-flow. A dual-thermocouple probe, consisting of two fine-wire thermocouples with 25 μm and 50 μm wire diameters, was used to determine a compensated turbulent gas temperature. A sensitivity analysis shows that temperatures resolved using this dual-thermocouple technique are less sensitive to changes in thermocouple bead size, therefore, uncertainty is greatly reduced even when soot deposition on the thermocouple bead occurs in sooty flames. Mean and root-mean square (rms) fluctuations of gas temperature were recorded in a two-dimensional plane across the flame centerline. The mean gas temperature monotonically decreases away from the flame centerline at most flame heights, except for 1 diameter above the burner, where a temperature dip is observed. The rms temperature peaks shift from the edge of the flame to the center as the height increases. This is due to the enhanced mixing between fuel and air, which is further shown using probability density functions of the local gas temperature. A systematic temperature dataset with high spatial resolution is established for sooty flames, which is valuable for future soot and radiation model validation.

Keywords: local gas temperature; dual-thermocouple technique; time constant; probability density function; validation dataset

1. Introduction

Fire modeling has become a critical tool in fire science, used in both research and applied design scenarios. Two large-eddy simulation (LES)-based models in particular are commonly used in the field, FireFOAM [1,2] and the Fire Dynamics Simulator (FDS) [3]. Fundamental physical

and chemical models are integrated into these computational codes to capture multi-physics, multi-scale fire dynamics including a combination of chemical reactions, turbulent mixing, thermal and fluid dynamics. In order to use these models for research or applied scenarios, validation must occur both for realistic scenarios and of underlying physical models used in simulations. In order to perform such validations, high accuracy experimental datasets are needed.

The gas-phase temperature serves as an important fire characteristic, as it provides a direct scalar comparison with computational results. However, the turbulent reactive flow field in fires makes it challenging to obtain time-resolved temperature information. To date, researchers have used thermocouples, thin-filament pyrometry, multi-color optical probes and coherent anti-Stokes Raman scattering (CARS) thermometry to measure local gas temperatures in various configurations. CARS [4] appears to be the most unobtrusive way to measure local gas temperature without modifying the flame; however, the complex experimental setup requires an extensive investment and considerable calibration. Thin-filament pyrometry has also been successfully applied on both a methanol pool fire and a blue whirl [5–7]; however, this technique is limited to soot-free flames which don't reflect most practical scenarios. Multi-color optical probes feature simultaneous soot volume fraction and temperature measurements, however only soot, not gas temperature can be detected [8]. Thermocouples, on the other hand, have been widely used for high temperature measurements [9–11]; however, physical and mathematical models need to be employed to account for the thermal inertia of the thermocouple bead under turbulent, fluctuating fire conditions.

Several methods have been proposed to compensate for the thermal inertial effect and reconstruct the true local temperature from raw thermocouple readings [12–21]. The frequency response of a thermocouple, in principle, is a first-order lag system and can be compensated for using a first-order coefficient, namely a time constant. For a steady combustion process, the mean time constant of a thermocouple bead can be determined using an electrical heating method [15]. However, the dramatic fluctuations in both temperature and velocity in a fire environment leads to a varying time constant, where use of a mean value might lead to both over- and under-compensation of temperature signals. Measurement of the instantaneous time constant in turbulent conditions can be extremely difficult as it is a function of the local temperature and velocity, requiring synchronized measurements [16]. Previously, a dual-thermocouple technique has been proposed to estimate the fluctuating time constant without direct measurement of velocity [17–19]. This technique relies on assumption of fixed bead sizes of the thermocouples, which may change in sooty environments, ultimately introducing large errors [17]. Further improvements of the dual-thermocouple technique show a possible application in sooty flames, as the instantaneous time constant can be estimated without assuming bead diameters, only incorporating diameters to compensate for radiant losses [20,21].

In this work, local gas temperature measurements of buoyant, turbulent, ethylene diffusion flames have been conducted using a dual-thermocouple (dual-TC) probe made with two type-S fine-wire thermocouples. In alignment with the IAFSS Working Group on Measurement and Computation of Fire Phenomena (i.e. the MaCFP Working Group) [22,23], the present work aims to provide a detailed temperature validation dataset for a MaCFP target test case. Medium-scale, 15 kW ethylene diffusion flames are produced using a 15.2 cm round water-cooled burner

with a controlled co-flow at FM Global's laboratory [8]. This test case is intended to provide a dataset to validate soot and radiation models in buoyant flames. The radiative characteristics, including radiant power distribution, local soot volume fraction and soot temperature under normal and reduced-oxygen conditions have been reported in [8]. Here, temperature measurements including local mean, root-mean square (rms) fluctuation, and probability distribution profiles are presented, which are necessary for future development of this validation dataset.

2. Experimental setup

A 15 kW buoyancy-driven turbulent diffusion flame is produced in a 1.22 by 1.22 m^2 wide, 1.83 m tall water-cooled enclosure [8], as shown in Fig. 1. Chemically pure ethylene (>99.9%) was fed through a mass flow controller to a 15.2 cm diameter round gas burner. Before reaching the burner surface, fuel passes through a honeycomb with a 0.32 cm cell size and 2 cm thickness followed by two layers of coarse and fine steel beads (with a 2.54 cm thick layer of 0.48 cm diameter beads and a 2.54 cm thick layer of 0.31 cm diameter beads, respectively) to assure a uniform exit flow velocity. Air co-flow is supplied through a rotameter with a mass flow rate of $52\ g/s$ and an uncertainty of $\pm\ 10\%$. Uniform air co-flow was achieved after passing through a plenum of fine screens and a 3.81 cm thick layer of sand. During each test, the water-cooled burner surface remains at about 353 K. More details of this setup are reported in [8].

The dual-TC pair was made with two type-S thermocouples, with 25 μm and 50 μm wire diameters (Omega Engineering, P10R-001 and P10R-002). The corresponding average bead diameters are measured as 88 μm and 126 μm, respectively, using a microscope. The thermocouple wires were supported by a single 1.6 mm diameter twin bore ceramic cylinder (Omega Engineering, TRX-164116) with a smaller ~8 mm length of thermocouple wire exposed. The beads of the dual-TC were positioned about 0.5 mm apart to ensure both thermocouples are exposed to nearly identical thermal field conditions. The validity of the identical surrounding condition assumption was tested using two identical thermocouples with 50 μm wire diameter. A 15 cm methanol pool fire was selected to minimize any affects caused by soot. The resultant cross-correlation coefficient of the signal fluctuations, $R_{12} = \overline{T'_{th1} T'_{th2}} / (\overline{T'^2_{th1}}\ \overline{T'^2_{th2}})^{1/2}$, has a value larger than 0.98, indicating that both thermocouples measure the same surrounding gas temperature.

During tests, a thermocouple rake using 8 pairs of dual-TCs with a 1-cm interval was traversed in a two-dimensional plane across the burner centerline by a stepper-motor driven X-Y axis with 10 μm accuracy. After putting in the thermocouple rake, the symmetry of the flame was ensured using averaged flame images over 60 s (recorded at 30 fps). Observation of the flame through the testing window was made for each experiment, no significant changes were observed to be introduced by the thermocouple rake. For the vertical direction, measurements were taken from 1.0*D* (*D* is the burner diameter) to 3.5*D* with a 0.5*D* interval, for the radial direction, measurements were taken from 0 cm at the flame centerline to 11 cm away from the centerline, with 1 cm intervals. Temperature signals, in μV, were digitally sampled at 5 kHz for 60 s at each

point. The voltage signals were converted to temperature using a NIST table [24] for type-S thermocouples. A cold junction correction was considered for all cases.

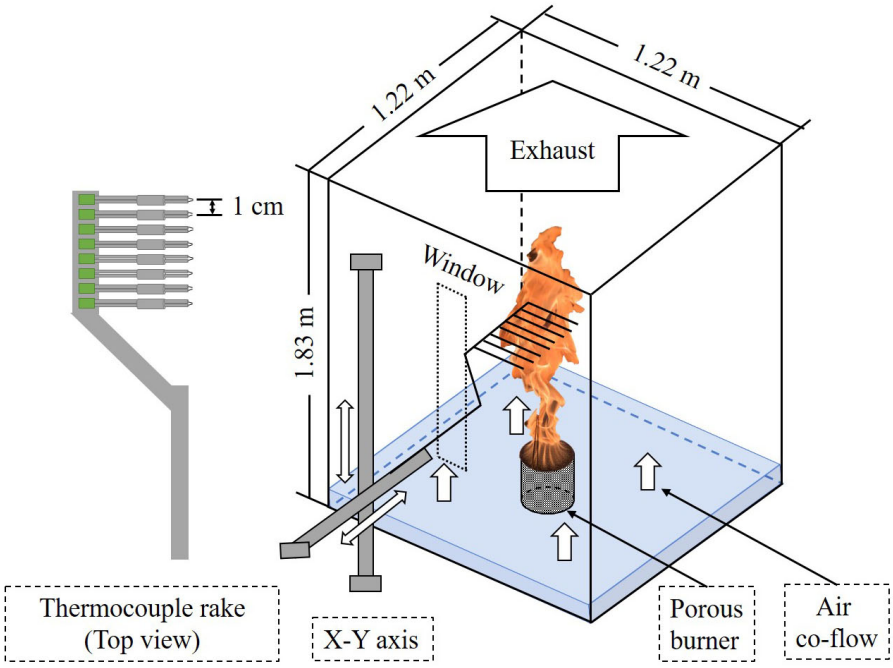

Fig. 1. Schematic of the experimental setup

3. Thermocouple compensation methods

Due to the thermal inertial of the thermocouple bead, high-frequency temperature fluctuations recorded by a micro thermocouple (typically with a wire diameter from 25 μm to 125 μm) are attenuated. In order to reconstruct local gas temperature, a time constant is needed to compensate the measured temperature. Both single and dual-thermocouple methods are discussed below to calculate the time constant.

3.1 Single-thermocouple method

A heat balance for a single thermocouple (Single-TC) bead under an unsteady turbulent flame with negligible conduction to lead wires can be written as

$$mc_p \frac{dT_{th}}{dt} = A\left[\left(T_g - T_{th}\right) * h - \varepsilon\sigma T_{th}^4 + \varepsilon \dot{q}''_{rad}\right], \quad (1)$$

where the left-hand side (LHS) of the equation represents the energy change of the thermocouple bead, m is the bead mass (kg), c_p is the bead heat capacity (J/kg · K), and T_{th} is the thermocouple bead temperature (K). The right-hand side (RHS) includes convective heating/cooling, radiant heat losses from the bead, and radiant heat absorption of bead from the surrounding fire, respectively. Heat absorption from the ambient air is sufficiently small and is ignored. Here, A is the bead area (m^2), T_g is the local gas temperature (K), h is the heat-transfer

coefficient ($\mathrm{W/m^2K}$), ε is the bead emissivity (assumed to be 0.95 for soot-coated bead), and $\dot{q}''_{rad}$ is the radiant heat flux ($\mathrm{W/m^2}$) from the surrounding fire. Eq. 1 can be re-written with T_g on the LHS,

$$T_g = T_{th} + \frac{V}{A}\frac{\rho c_p}{h}\frac{dT_{th}}{dt} + \frac{1}{h}(\varepsilon\sigma T_{th}^4 - \varepsilon\dot{q}''_{rad}) \tag{2}$$

where h can be calculated as $\mathrm{Nu}k_g/d$, with Nu representing the Nusselt number, k_g being the temperature-dependent thermal conductivity ($\mathrm{W/mK}$) of gas, and d being the thermocouple bead diameter (m). Further, V/A represents the inverse of a surface to volume ratio of a thermocouple bead and ρ is the bead density ($\mathrm{kg/m^3}$). According to observations of thermocouples used in this study using a microscope, a spherical structure is assumed for the thermocouple beads, providing $V/A = d/6$. In some previous studies a cylindrical structure is also used [13,20], resulting in $V/A = d/4$. Substituting the above parameters into Eq. 2 provides

$$T_g = T_{th} + \frac{\rho c_p d^2}{6\mathrm{Nu}k_g}\frac{dT_{th}}{dt} + \frac{d}{\mathrm{Nu}k_g}(\varepsilon\sigma T_{th}^4 - \varepsilon\dot{q}''_{rad}), \tag{3}$$

where

$$\mathrm{Nu} = 2 + 0.6\mathrm{Re}^{1/2}\mathrm{Pr}^{0.4} \tag{4}$$

and

$$\tau = \frac{\rho c_p d^2}{6\mathrm{Nu}k_g}. \tag{5}$$

Using a Nu correlation for flow around a sphere [25] from Eq. 4, where Re is the Reynolds number (Ud/ν, where ν is the kinematic viscosity of the fluid in $\mathrm{m^2/s}$), and Pr is the Prandtl number (ν/α, where α is the thermal diffusivity of the fluid in $\mathrm{m^2/s}$), the time constant can be calculated using Eq. 5 [20,25], ultimately becoming a strong function of local gas velocity, temperature and bead diameter, i.e. $\tau = f(U, T_g, d)$. The local gas temperature in Eq. 3 can then be solved after accounting for any additional external $\dot{q}''_{rad}$.

In practice, the complex geometry of the thermocouple bead and wire combination leads to large uncertainties in bead diameter. Especially for sooty flames, soot deposits on the thermocouple bead due to thermophoresis and leads to growth of the bead size throughout the duration of measurements. To determine the influence of this phenomena on measured temperatures and response rates, a sensitivity and uncertainty study was conducted. A temperature signal sampled in the flame centerline at a height of $2.5D$ was used. Normalized sensitivity $s(T_{g,i})$ and absolute uncertainty values $u(T_{g,i})$ were calculated using following equations [26,27],

$$s(T_{g,i}) = \frac{x_i}{T_{g,i}}\frac{\partial T_{g,i}}{\partial x_i} \tag{6}$$

$$u\big(T_{g,i}\big) = \Delta x_i \frac{\partial T_{g,i}}{\partial x_i}, \tag{7}$$

where x_i is the input variable at step i and Δx_i is the uncertainty of any input parameter x_i.

Fig. 2(a) shows the sensitivities of the time-resolved compensated T_g signal to the measured parameters. We can see T_g is very sensitive to the original thermocouple output temperature T_{th}

and bead diameter d, and less sensitive to the local gas velocity U and radiant heat flux $\dot{q}''_{rad}$. In experiments, the relative uncertainty of T_{th} is relative small, estimated to be 0.25% for a type-S thermocouple and associated data acquisition system, thus the overall T_g uncertainty is $\pm$ 10 K within a 95% confidence interval (CI) in the flame, shown in Fig. 2(b). For velocity measurements, a 1.4 m/s flow velocity has been used based on previous measurement at FM Global using particle image velocimetry (PIV). A 20% measurement uncertainty is assigned in this analysis due to the fluctuating fire environment, with a resulting uncertainty of $\pm$ 14 K at 95% CI. For a small thermocouple bead, the effect of radiant heat flux on the temperature correction can usually be ignored. In the present work, with a 15 kW ethylene flame approximately 0.7 m in height and 0.152 m in diameter, the radiant heat flux to a thermocouple bead at the flame centerline and a height of 2.5D, may be as high as 45 kW/m^2, see Appendix A. This external radiant heat flux results in an uncertainty ranging from -28 K to -16 K in a 95% CI for the 25 μm diameter wire (88 μm bead diameter). The bead diameter, on the other hand, is conservatively estimated to change only 20%, even though soot deposition may cause even more significant changes. The resulting uncertainty reaches – 199 K to 297 K in a 95% CI. The preceding analysis demonstrates that the single-TC compensation method is most sensitive to thermocouple bead diameter, with inaccurate bead size measurements leading to large temperature uncertainty, which may be exacerbated in sooty flames.

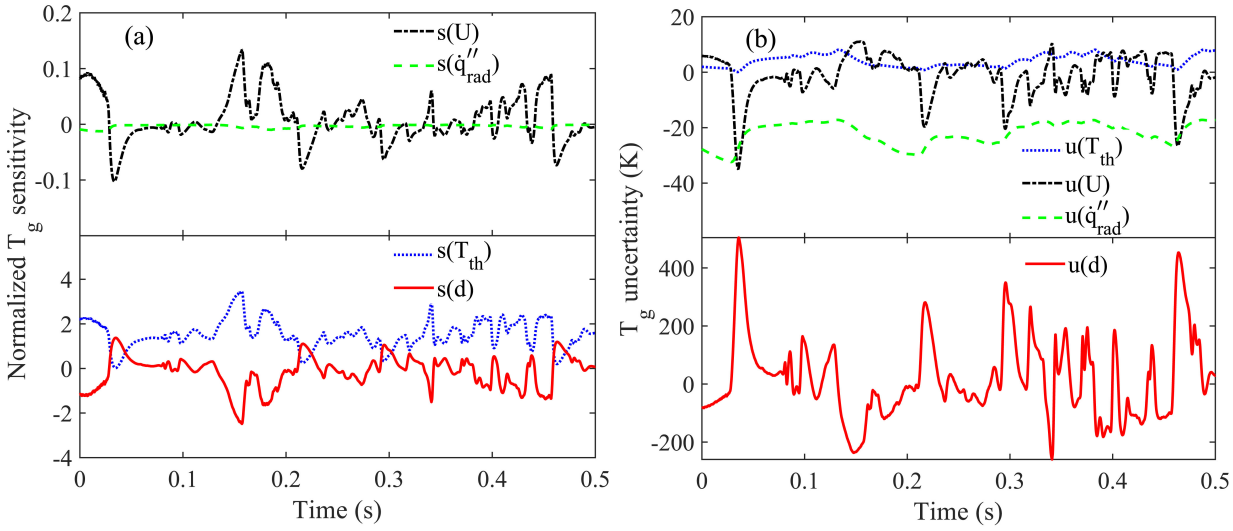

Fig. 2. Time-resolved sensitivities (s) and uncertainties (u) of single-TC method: (a) Normalized T_g sensitivities, (b) Absolute T_g uncertainties.

3.2 Dual-thermocouple method

A dual-thermocouple (Dual-TC) method has been proposed by Tagawa and Oath [20] to compensate the local gas temperature which is less affected by the geometrical features of the thermocouple beads. The basic assumption is that, by putting two fine-wire thermocouple beads close together, typically less than 0.5 mm, both thermocouples are under identical surrounding conditions. The following two equations are then formed for two thermocouples,

$$T_{g1} = T_{th1} + \tau_1\left(\frac{dT_{th1}}{dt} - \frac{6}{\rho c_p}\left(\frac{\varepsilon \dot{q}''_{rad} - \varepsilon\sigma T_{th1}^4}{d_1}\right)\right) \quad (8)$$

$$T_{g2} = T_{th2} + \tau_2\left(\frac{dT_{th2}}{dt} - \frac{6}{\rho c_p}\left(\frac{\varepsilon \dot{q}''_{rad} - \varepsilon\sigma T_{th2}^4}{d_2}\right)\right), \quad (9)$$

where the subscripts 1 and 2 denote two thermocouples with diameters of d_1 (88 μm) and d_2 (126 μm), respectively. Assuming identical surrounding conditions,

$$T_{g1} = T_{g2} = T_g, \quad (10)$$

which implies that both compensated temperatures should equal the true local gas temperature. Equation 10 holds true for all temperature pairs; therefore, the problem is reduced to finding τ_1 and τ_2 to satisfy Eq. 10 for temperature pairs measured at all times. Assuming there are a total of N pairs of measurements, Eq. 8 and Eq. 9 can be solved for by finding τ_1 and τ_2 to minimize Eq. 11 using a least-squares method

$$e = \frac{\sum_1^N |T_{g1} - T_{g2}|}{N}. \quad (11)$$

The duration over which N pairs of temperature signals are acquired is defined as the time window. In order to include sufficient data points to evaluate τ_1 and τ_2, a time window needs to be selected that is large enough to reflect the heat transfer process but, ideally, small enough to resolve turbulent fluctuations. Selection of a time window that is too short may result in unrealistic time constants. Previous literature [20,21] suggest a time window selection between 1.5 ~ 3.0 times of the mean time constant of the thinner thermocouple. In the present work, a 0.06 s (~$4\bar{\tau}_1$, where $\bar{\tau}_1$ is the mean time constant of the 25 μm wire thermocouple) time window was used. The mean time constant $\bar{\tau}_1$ was obtained through use of all temperature data points with a least squares method (i.e. a 60 s signal with a 5 kHz sampling rate, totaling 300,000 data points).

The advantage of this dual-TC scheme is that the thermocouple bead diameters are only used to calculate the radiant loss term, which results in less uncertainty. Measured velocities are no longer needed, which makes the experiments more convenient and cost effective. Sensitivity and uncertainty analyses were conducted to evaluate the effect of the bead diameter. Fig. 3(a) shows the sensitivities and uncertainties of the two thermocouple beads. Compared with the single-TC method, T_g is much less sensitive to the bead diameter. A 20% increase in diameter leads to only a – 25 K to 8 K uncertainty at a 95% CI, which is much less than the uncertainties induced by the single TC method. The temperature compensation contributed by different terms in Eq. 8 is plotted in Fig.3(b). As shown, the most important term is $\tau\,(dT_{th}/dt)$, which represents the contribution of convective heating, while the radiant heat loss term, $\tau(6\varepsilon\sigma T_{th}^4/\rho c_p d)$, plays a secondary role. For the radiant absorption term, $\tau(-6\varepsilon\dot{q}''_{rad}/\rho c_p d)$, a 45 kW/m^2 heat flux leads to a temperature compensation ranging from – 31 K to -2 K in a 95% CI. Considering the uncertainties caused by a 0.25% data acquisition error, a 20% bead size change, and a 45 kW/m^{2}external radiant heat flux, the overall uncertainty on the compensated local hot gas temperature T_g was estimated at ± 41 K.

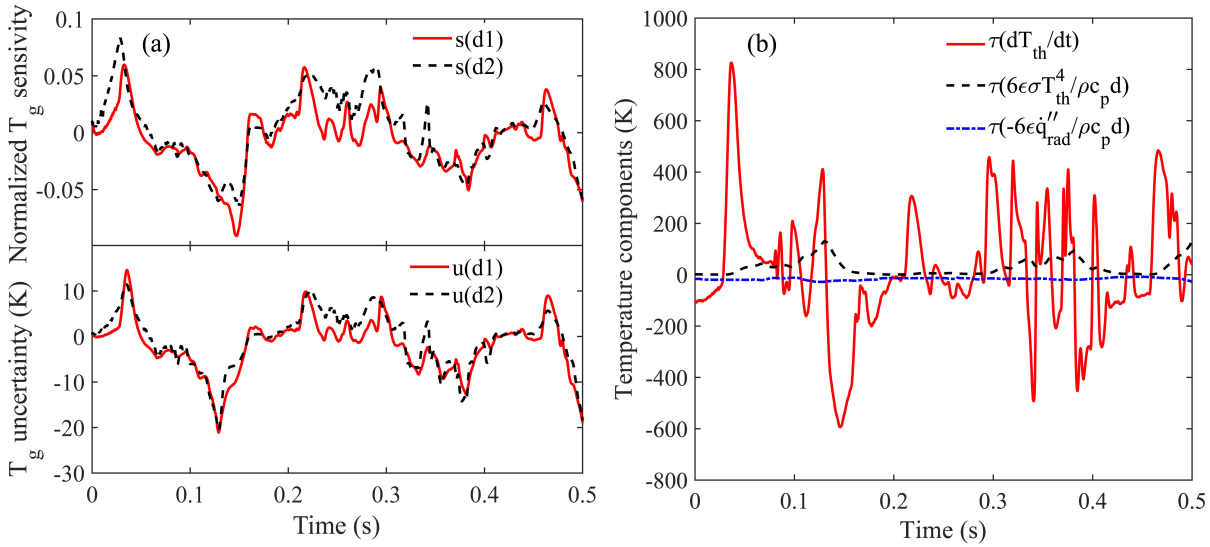

Fig. 3. (a) Time-resolved sensitivities and uncertainties on thermocouple bead diameter of dual-TC methods, (b) Time-resolved temperature compensation components on a 25 μm wire diameter TC

4. Results and discussion

4.1 Compensated temperature signal

Fig. 4(a) shows an example of a 1 s duration of compensated temperatures and the corresponding fluctuating time constants along the flame centerline at a height of 2.5D. Uncompensated temperatures from the 25 µm wire diameter TC, T_{th1} show a higher sensitivity and wider temperature range than the 50 µm wire diameter T_{th2} measurements due to its smaller thermal inertia. Although both T_{th1} and T_{th2} reflect fluctuations in the flow field, details, especially in higher and lower temperature ranges, are missing (T_{th1}: 400 ~ 1770 K, T_{th2}: 620 ~ 1280 K). In comparison, the compensated temperature signals T_{g1} and T_{g2} show good agreement, with a cross-correlation coefficient around 0.99. Compensated temperature fluctuations with a higher frequency resolution show a broader temperature range, from 300 K ~ 2100 K, where the lower and upper limits correspond to the ambient air temperature and flame temperature of ethylene, respectively. The maximum temperature in a turbulent ethylene diffusion flame should be less than the adiabatic flame temperature of ethylene, i.e. 2370 K, primarily due to radiant losses. A power spectral density analysis shows that the compensated temperature signal has a frequency up to 600 Hz, which is able to resolve a majority of the gas temperature fluctuations shown in Fig. 4(a).

The computed time constants are shown in Fig. 4(b). Both time constant signals fluctuate with changes in the surrounding flow field and follow the same trend. The 25 µm wire thermocouple has a smaller fluctuating time constant, with a mean value of 0.015 s, while for the larger wire diameter the time constant is 6 to 7 times larger.

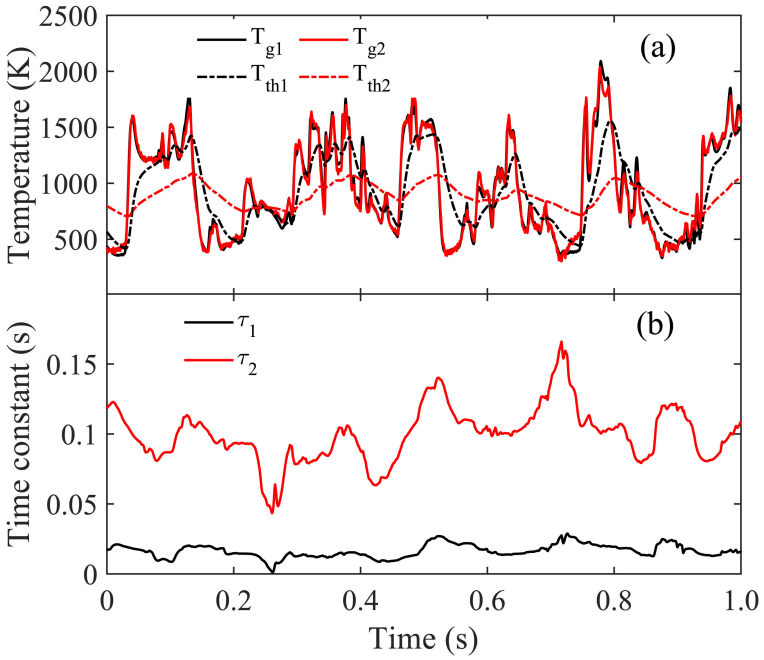

Fig. 4. Time resolved compensated temperature and time constants at the flame centerline and a height of 2.5*D*: (a) raw and compensated gas temperature, (b) calculated fluctuating time constants.

Auto-correlation of the temperature signals shows this flame has a Taylor-micro time scale ranging from 0.02 to 0.04 s, from the centerline to the outer edge of the flame. Assuming a 1.4 m/s centerline vertical gas velocity at a height of 2.5*D* above the burner, as well as Taylor's frozen turbulence hypothesis, the Taylor microscale at the flame centerline is calculated to be ~ 0.028 m. Weckman [16] previously investigated the turbulent structures of a 31 cm diameter methanol pool fire, similar to the flame in the present work (i.e. a turbulent Reynolds number from 100 to 200). Their results show the ratio of Taylor to Kolmogorov time scales is around 2.5:1 at the central core of the fire and 8:1 at the edges of the fire. (For comparison, the ratio of Taylor to Kolmogorov length scales in an isothermal, fully developed, plane, momentum-dominated jet is on the order of 70 [28].) This leads to an estimated Kolmogorov length scale ranging from around 10 mm to 0.4 mm and a time scale ranging from 0.005 to 0.008 s, for the current 15 kW ethylene flame at 2.5*D* in height. In this study, the spatial distance between the thermocouple beads is around 0.5 mm and the time constant for the thinner thermocouple is around 0.015 s, which are comparable with the estimated Kolmogorov length scales. This analysis, however, is still a rough estimation. Further velocity measurements are needed for a detailed discussion.

4.2 Flame centerline temperature

Fig. 5(a) shows the mean, rms and ratio between rms and mean temperatures, i.e. the coefficient of variation (CV), along the centerline of the flame. The mean temperature reaches a maximum value at a height of 1.5*D*, followed by a slight decrease until 2.5*D*, after which the mean

temperature drops due to the end of the flame region; similar results have been reported in the literature [16,29]. The rms temperature fluctuations show a different trend, which increases from a height of 1.0D with a maximum value at 2.5D. The CV, $T_{g,rms}/T_{g,mean}$, follows a similar trend with the rms temperature, but with a maximum value at a height of 3.0D.

Probability density function (PDF) profiles of temperature are presented as a function of height in Fig. 5(b). At a height of 1.0D, the temperature PDF shows a single peak distribution with a temperature value around 1100 K at the maximum probability and a reduced temperature probability under 600 K. This occurs because, at a height of 1.0D, a narrow necking region is present between intermittent 'puffs' of the flame, as shown in Fig. 5(c), where the flame is less turbulent and relatively steady. Insufficient mixing of fuel and air results in less frequency of flame occurrence, and thus a lower mean and rms temperature. As height increases, buoyancy-driven turbulence gradually increases, enhancing mixing between fuel and air. Lower temperatures from 300 K to 600 K are evident in PDF profiles at heights of 1.5D to 2.5D, meanwhile, PDF profiles shift toward larger values and temperatures higher than 2000 K are detected. This broader temperature distribution leads to a higher rms temperature. At a height of 3.0D, the PDF profile shows a bi-modal distribution, with the upper temperature limits shifting back to a lower value. This is attributed to the combination of fuel burn out and increased air entrainment in this region. For larger heights of 3.5D, the flame is more intermittent and hot burnt gases and air dominate. The PDF profile again shows a single peak distribution with a much lower peak temperature.

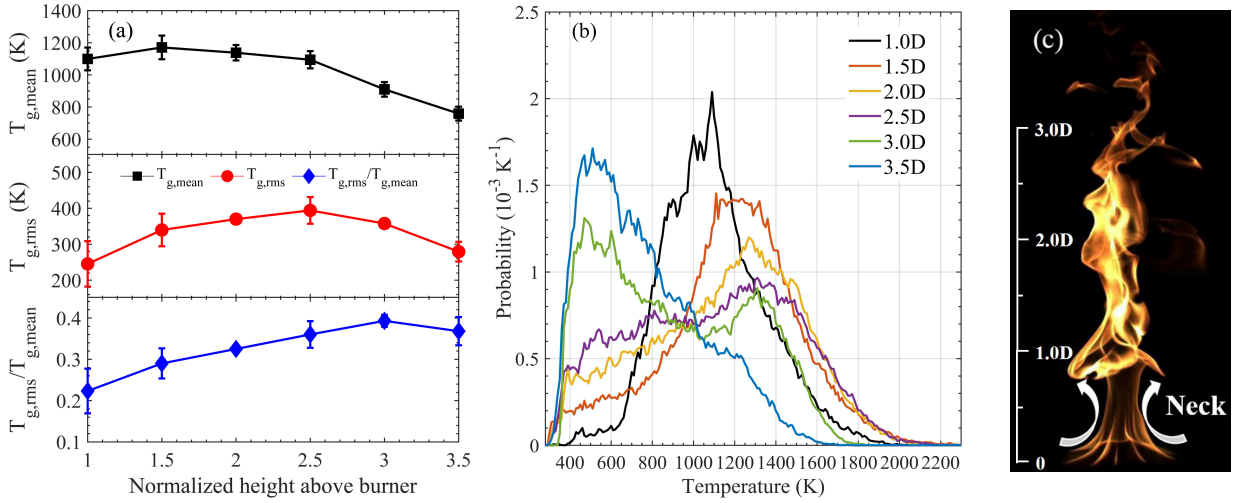

Fig. 5. Flame centerline temperatures at different heights: (a) mean, rms and ratio of rms and mean temperatures, (b) PDF profiles of temperature, (c) image of the flame. Note the necking of the flame at the base which is responsible for significant mixing and variability at the base.

4.3 Overall temperature statistics

To have a better understanding of the overall flame structure, the mean and rms temperature distributions in a two-dimensional plane across the flame centerline were measured, as shown in Fig. 6, where the error bar represents the standard deviation between 2 to 3 repeated

measurements. For a height of 1.0*D*, a dip in the mean temperature at the flame centerline (r = 0 ~ 1 cm) is consistently observed. This same trend was also observed by Weckman et al. [16] for methanol pool fires. As discussed before, fuel-rich conditions at this location lead to lower mean and rms temperatures. Away from the centerline, enhanced mixing between fuel and air results in increased mean and rms temperatures. From 1.5*D* to 3.5*D*, the mean temperature monotonically decreases moving away from the centerline in the radial direction, with the peak mean temperature near 1200 K. The peak rms temperature fluctuates around 400 ~ 425 K and is observed 4 cm away from the centerline at 1.0*D*. This is consistent with the necking behavior shown in Fig. 5(c), where intense mixing occurs in this region away from the flame centerline. As the height increases, the location of the peak rms temperature moves toward the centerline of the flame. After a height of 2.5*D*, the peak rms temperature is located at the flame centerline.

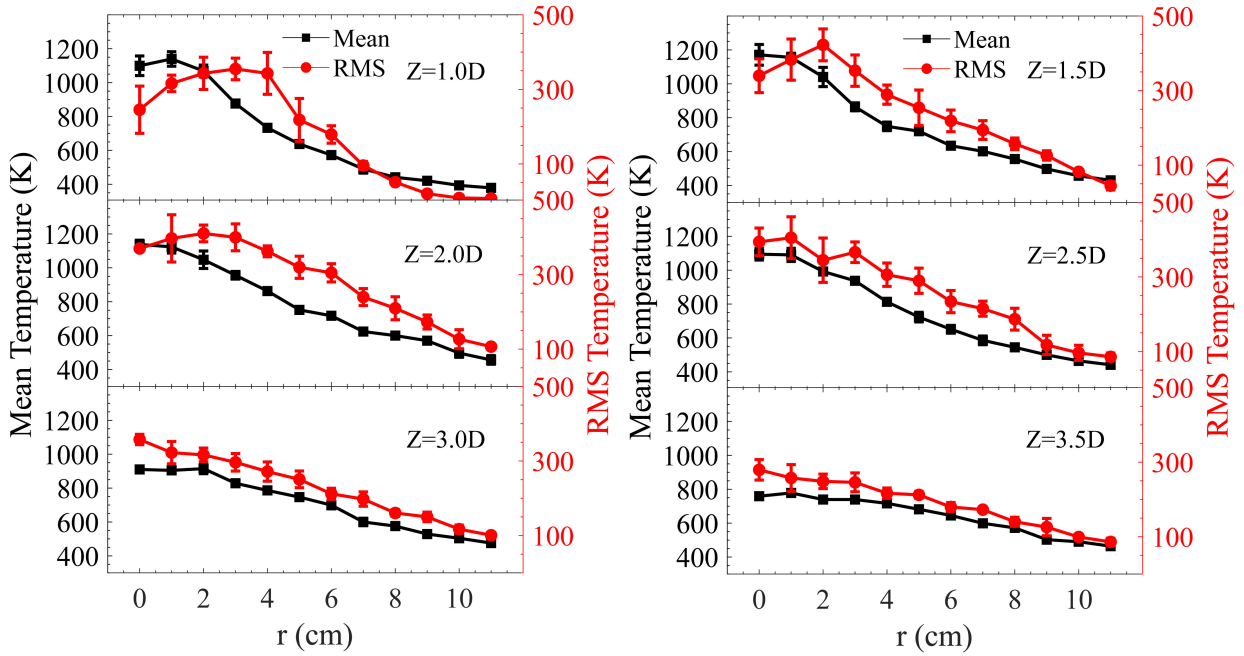

Fig. 6. Mean and rms temperatures at different heights and radial locations

Temperature PDF profiles in both horizontal (0 to 4 cm) and vertical directions are plotted in Fig. 7. At a height of 1.0*D*, there is a large probability of high temperatures, i.e. >1200 K, at $r =$ 2 cm, showing good mixing between fuel and air; inward from this location, the environment tends to be fuel rich. For the outward direction, the PDF shifts to a lower value due to increased penetration of ambient air. PDF profiles at a height of 1.5*D* have a similar trend with those at 1.0*D,* except the probability of air entrainment into the centerline region increases, promoting better mixing compared to the 1.0*D* location. From heights of 2.0*D* to 3.5*D*, PDF profiles become similar in the radial direction. A relatively homogeneous region is observed and enlarged from 0 ~ 2 cm at a height of 2.0*D* to 0 ~ 4 cm at 3.0*D*. The maximum temperature decreases from near 2050 K to 1700 K. After a height of 3.0*D*, fuel burn out leads to a narrower temperature range and finally results in single peak distribution at 3.5*D* mainly corresponding to burnt gas. The probability at high temperatures (i.e. 2000 ~ 2050 K) is relatively low, around

5.0E-5 K^{-1} from 1.0*D* to 2.5*D* near the flame centerline. As a comparison, Kearney et al [4] measured the temperature profile of a 2-m diameter turbulent pool fire with a 10%-toluene/90%-methanol fuel using the CARS technique. Their results show that at heights of 0.5 to 1.5 m, the temperature probability at 2000 ~ 2050 K has a value ranging from 2E-4 to 4E-4. The discrepancy on the high temperature probability might be attributed to the different fuels and fire sizes used in these two works. A possible explanation for this low probability at higher temperatures is that a large amount of air entrainment leads to a sparse presence of the flame sheet in this turbulent flame.

Overall, starting from 1.0*D* at the flame centerline, mixing between fuel and air is enhanced both horizontally and vertically with a corresponding increase in probability of high temperatures, e.g. the presence of the flame. At the base of the flame, large vortical structures form which oscillate within the necking flame region. As the flame evolves upward, flow instability increases, and vortex structures break down into smaller vortices, promoting mixing between fuel and air and leading to increased mean gas temperatures. Further upward, the combined effects of buoyancy-induced turbulence development and fuel burnout result in homogeneous burning with a reduced mean temperature.

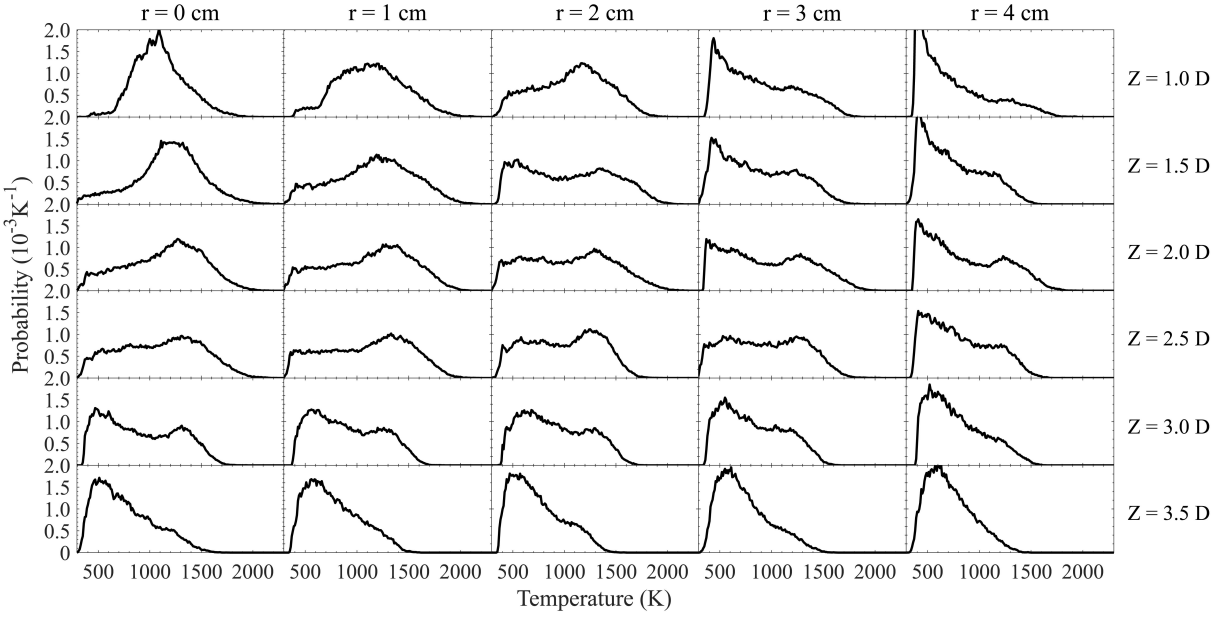

Fig. 7. Temperature probability distribution at different locations

5. Conclusions

A dual-thermocouple technique has been applied to a carefully-instrumented turbulent ethylene diffusion flame in order to provide accurate gas temperature measurements. Both sensitivity and uncertainty analyses show that this improved dual-TC technique has advantages under hostile flame environments where the bead diameter may change due to soot deposition or other effects.

Measured temperatures were compensated using a temporally-varying time constant, producing a systematic temperature validation dataset for 15 kW buoyant turbulent ethylene flames useful for future model development and validation. The resultant mean, rms and PDF temperature profiles provide a detailed picture of the turbulent flame structure.

These temperature measurements, alongside existing data such as the radiant power distribution, local soot volume fraction and soot temperature, as well as future gas velocity measurements will provide a detailed dataset of this flame for validation and development of radiation models. This data is still limited to the 15 kW ethylene diffusion flame investigated. Future applications of the dual-thermocouple technique on different fuels and fire sizes, i.e. a soot-free flame and a larger fire, are needed to improve our understanding of turbulent buoyant flames.

Acknowledgements

The authors would like to acknowledge financial support for this work from FM Global and the National Science Foundation through CBET award 1554026 and the INTERN program. The authors would also like to thank Robert Tabinowski, Aaron Cunha and Gennadiy Geyyer of FM Global for their efforts in conducting the experiments.

Appendix A.

Radiant heat flux estimation

The heat flux to a thermocouple bead can be estimated by assuming the thermocouple bead has a diameter of $d_i, i = 1,2$. The fire is idealized to have a cylindrical shape, with a height of $z_f =$ 0.7 m, and diameter of $d_f = 0.152$ m. The radiative power per unit volume of the fire ($\mathrm{kW/m^3}$) is

$$\dot{q}_r''' = \frac{Q}{V_f}\chi_r, \tag{A.1}$$

where Q is the theoretical heat-release rate (15 kW), V_f is the flame volume ($z_f \pi d_f^2/4$), and χ_r is the radiant fraction (0.34 for ethylene).

Fig. A.1 shows a thermocouple placed at a radius of r_{th} and a height of Z_{th}. For an infinitely-small flame volume element at a height of z_0, radius of r_0 from the centerline, and an azimuthal angle of θ degree from *x* axis, the distance of the element to thermocouple is

$$d_{th-f} = \{[(r_{th} + r_0)\sin(\theta/2)]^2 + [(r_{th} - r_0)\cos(\theta/2)]^2 + (z_0 - z_{th})^2\}^{1/2}. \tag{A.2}$$

The radiant heat flux per unit area to the surface of the thermocouple is

$$q_{r,u}'' = \int_0^{d_f/2}\int_0^{Z_f}\int_0^{2\pi} \frac{r_0 \dot{q}_r'''}{4\pi d_{th-f}^2}\, d\theta\, dz_0 dr_0. \tag{A.3}$$

Using Eq. A.3, $\dot{q}_{rad}''$ for a thermocouple can be determined. The highest possible heat flux is determined at the center location (0 cm radius, 2.5*D*=0.38 m height), with $\dot{q}_{rad}'' = 45\ \mathrm{kW/m^2}$.

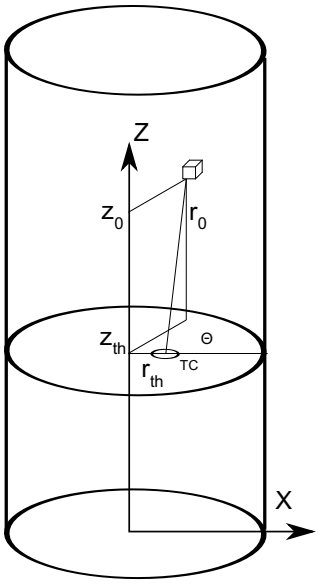

Fig. A.1 Idealized flame radiant heat flux calculation.

6. References

[1] FM Global, FireFOAM, Available from: http://www.fmglobal.com/modeling

[2] Y. Wang, P. Chatterjee, J.L. De Ris, Large eddy simulation of fire plumes, Proc. Combust. Inst. 33 (2011) 2473–2480. doi:10.1016/j.proci.2010.07.031.

[3] K. McGrattan, S. Hostikka, R. McDermott, J. Floyd, M. Vanella, Fire Dynamics Simulator User's Guide, NIST Spec. Publ. 1019 Sixth Ed. (2019) 347. doi: 10.6028/NIST.SP.1019.

[4] S.P. Kearney, T.W. Grasser, Laser-diagnostic mapping of temperature and soot statistics in a 2-m diameter turbulent pool fire, Combust. Flame. 186 (2017) 32–44. doi:10.1016/j.combustflame.2017.07.018.

[5] Z. Wang, W.C. Tam, K.Y. Lee, A. Hamins, Temperature Field Measurements using Thin Filament Pyrometry in a Medium-Scale Methanol Pool Fire - NIST Technical Note 2031, (2018). doi:10.6028/NIST.TN.2031.

[6] S.B. Hariharan, E.T. Sluder, M.J. Gollner, E.S. Oran, Thermal structure of the blue whirl, Proc. Combust. Inst. 37 (2019) 4285–4293. doi:10.1016/j.proci.2018.05.115.

[7] S.B. Hariharan, P.M. Anderson, H. Xiao, M.J. Gollner, E.S. Oran, The blue whirl: Boundary layer effects, temperature and OH* measurements, Combust. Flame. 203 (2019) 352–361. doi:10.1016/j.combustflame.2019.02.018.

[8] D. Zeng, P. Chatterjee, Y. Wang, The effect of oxygen depletion on soot and thermal radiation in buoyant turbulent diffusion flames, Proc. Combust. Inst. 37 (2019) 825–832. doi:10.1016/j.proci.2018.05.139.

[9] G. Cox, R. Chitty, A study of the deterministic properties of unbounded fire plumes,

Combust. Flame. 39 (1980) 191–209. doi:10.1016/0010-2180(80)90016-4.

[10] O. Korobeinichev, M. Gonchikzhapov, A. Tereshchenko, I. Gerasimov, A. Shmakov, A. Paletsky, A. Karpov, An experimental study of horizontal flame spread over PMMA surface in still air, Combust. Flame. 188 (2018) 388–398. doi:10.1016/j.combustflame.2017.10.008.

[11] S. Brohez, C. Delvosalle, G. Marlair, A two-thermocouples probe for radiation corrections of measured temperatures in compartment fires, Fire Saf. J. 39 (2004) 399–411. doi:10.1016/j.firesaf.2004.03.002.

[12] W.C. Strahle, M. Muthukrishnan, Thermocouple time constant measurement by cross power spectra, AIAA J. (1976). doi:10.2514/3.7268.

[13] M. Vachon, P. Cambray, T. Maciaszek, J.C. Bellet, Temperature and velocity fluctuation measurements in a diffusion flame with large buoyancy effects, Combust. Sci. Technol. 48 (1986) 223–240. doi:10.1080/00102208608923894.

[14] S.J. Fischer, B. Hardouin-Duparc, W.L. Grosshandler, The structure and radiation of an ethanol pool fire, Combust. Flame. 70 (1987) 291–306. doi:10.1016/0010-2180(87)90110-6.

[15] M. Kunugi, H. Jinno, Measurements of fluctuating flame temperature, Symp. (Int.) Combust. 7 (1958) 942–948. doi:10.1016/S0082-0784(58)80141-1.

[16] E.J. Weckman, A.B. Strong, Experimental investigation of the turbulence structure of medium-scale methanol pool fires, Combust. Flame. 105 (1996) 245–266. doi:10.1016/0010-2180(95)00103-4.

[17] A. Ballantyne, J.B. Moss, Fine wire thermocouple measurements of fluctuating temperature, Combust. Sci. Technol. 17 (1977): 63-72. doi:10.1080/00102209708946813.

[18] L.J. Forney, G.C. Fralick, Two-wire thermocouple: Frequency response in constant flow, Rev. Sci. Instrum. 66 (1995) 3331–3336. doi:10.1063/1.1145503.

[19] P.G. O'Reilly, R.J. Kee, R. Fleck, P.T. McEntee, Two-wire thermocouples: A nonlinear state estimation approach to temperature reconstruction, Rev. Sci. Instrum. 72 (2001) 3449–3457. doi:10.1063/1.1384428.

[20] M. Tagawa, Y. Ohta, Two-thermocouple probe for fluctuating temperature measurement in combustion - Rational estimation of mean and fluctuating time constants, Combust. Flame. 109 (1997) 549–560. doi:10.1016/S0010-2180(97)00044-8.

[21] P.A. Santoni, T. Marcelli, E. Leoni, Measurement of fluctuating temperatures in a continuous flame spreading across a fuel bed using a double thermocouple probe, Combust. Flame. 131 (2002) 47–58. doi:10.1016/S0010-2180(02)00391-7.

[22] B. Merci, A. Trouvé, Call for participation in the second workshop organized by the IAFSS Working Group on, Fire Saf. J. 105 (2020) 92–94. doi:10.1016/j.firesaf.2019.02.010.

[23] A. Brown, M. Bruns, M. Gollner, J. Hewson, G. Maragkos, A. Marshall, R. McDermott, B. Merci, T. Rogaume, S. Stoliarov, J. Torero, A. Trouvé, Y. Wang, E. Weckman, Proceedings of the first workshop organized by the IAFSS Working Group on

Measurement and Computation of Fire Phenomena (MaCFP), Fire Saf. J. 101 (2018) 1–17. doi:10.1016/j.firesaf.2018.08.009.

[24] M.C. Croarkin, W.F. Guthrie, G.W. Burns, M. Kaeser, G.F. Strouse, Temperature-Electromotive Force Reference Functions and Tables for the Letter-Designated Thermocouple Types Based on the ITS-90, Natl. Inst. Stand. Technol. Monogr. 175. (1993).

[25] C.R. Shaddix, Correcting Thermocouple Measurements for Radiation Loss: A Critical Review, Proceedings of the 33rd National Heat Transfer Conference, Albuquerque, New Mexico, August 15–17, 1999.

[26] B.N. Taylor, C.E. Kuyatt, NIST Technical Note 1297 1994 Edition Guidelines for Evaluating and Expressing the Uncertainty of NIST Measurement Results NIST Technical Note 1297 1994 Edition Guidelines for Evaluating and Expressing the Uncertainty of NIST Measurement Results, (1994).

[27] V. Gururajan, F.N. Egolfopoulos, Direct sensitivity analysis for ignition delay times, Combust. Flame. 209 (2019) 478–480. doi:10.1016/j.combustflame.2019.08.007.

[28] E. Gutmark, I. Wygnanski, The planar turbulent jet, J. Fluid Mech. 73 (1976) 465–495. doi:10.1017/S0022112076001468.

[29] B.J. McCaffrey, Purely buoyant diffusion flames: some experimental results, NBSIR 79-1910, 1979. doi:NBSIR 79-1910.